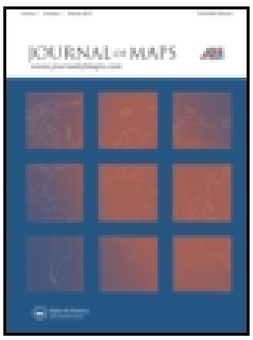

Journal of Maps

ISSN: (Print) 1744-5647 (Online) Journal homepage: https://www.tandfonline.com/loi/tjom20

# Structural geology of Ganymede regional groove systems (60°N–60°S)

Costanza Rossi, Paola Cianfarra & Francesco Salvini

**To cite this article:** Costanza Rossi, Paola Cianfarra & Francesco Salvini (2019): Structural geology of Ganymede regional groove systems (60°N–60°S), Journal of Maps, DOI: 10.1080/17445647.2019.1685605

**To link to this article:** https://doi.org/10.1080/17445647.2019.1685605

JOURNAL OF MAPS
https://doi.org/10.1080/17445647.2019.1685605

Taylor & Francis
Taylor & Francis Group

Science



# Structural geology of Ganymede regional groove systems (60°N–60°S)

Costanza Rossi, Paola Cianfarra and Francesco Salvini

GeoQuTe Lab, Science Department, Roma Tre University, Rome, Italy

**ABSTRACT**

Brittle deformation on Ganymede surface is represented by grooves tectonic linear landforms. These are regional scale structures that show well-defined morphology from straight to curvilinear. High density of grooves occupies most of the light terrain of the satellite, the grooved terrain. We map grooves on the USGS Voyager and Galileo Mosaic of Ganymede in order to unravel their spatial distribution and tectonic setting. A total of 14,707 grooves were identified, digitized and statistically analysed. A quantitative structural geology approach was used to classify grooves, by considering their azimuth and regional rotation. This procedure allowed to recognize a total of four groove families, named the NE, WNW, NW, and N-S super-systems. The presented structural map represents a tool to study the stress conditions associated with the groove formation and evolution. This map also aims to contribute to the scientific preparation of the upcoming missions and future exploration of Ganymede.

**ARTICLE HISTORY**
Received 7 May 2019
Revised 18 October 2019
Accepted 18 October 2019

**KEYWORDS**
Ganymede; tectonics; planetary geology; remote sensing; cartography

## 1. Introduction

Planetary missions successfully have been exploring the Outer Solar System for the last decades (e.g. Pioneer, Voyager, Galileo and Cassini–Huygens programmes, Fimmel, Van Allen, & Burgess, 1980; Matson, Spilker, & Lebreton, 2003; Smith et al., 1979a; Young, 1998). Their discoveries provided information on the gas giant planets and their moons. Ganymede is one of the icy satellites of the Jovian System and represents a primary target for planetary exploration. It is a candidate for habitability as a potential world that hosts life (Grasset et al., 2013; Prieto-Ballesteros, Bonales, & Munoz-Iglesias, 2012; Vance et al., 2018). It is the largest satellite in the Solar System with a radius of 2631.2 ± 1.7 km (Anderson et al., 2001) and presents the lowest moment of inertia (0.3115 ± 0.0028; Anderson, Lau, Sjogren, Schubert, & Moore, 1996; Hussmann, Sotin, & Lunine, 2007; Schubert, Anderson, Spohn, & McKinnon, 2004) as provided by gravity data and confirmed by geophysical models (e.g. Kirk & Stevenson, 1987). This implies a highly differentiated internal structure constituted by a metal-rich core and a silicate mantle surrounded by a water-ice crust (Anderson et al., 1996; Deschamps & Sotin, 2001; Schubert, Turcotte, & Olson, 2001; Sohl, Spohn, Breuer, & Nagel, 2002). The icy crust is composed by ice-Ih, ice-III, ice-V, and ice-VI. A liquid water layer is inferred to be located between ice-Ih and the high-pressure ice layers (i.e. ice-III; Hussmann et al., 2007). This water layer constitutes a subsurface ocean (Carr et al., 1998; Fanale, Johnson, & Matson, 1977; Khurana et al., 1998; Kirk & Stevenson, 1987; Kivelson et al., 2000; Moore & Schubert, 1996; Ojakangas & Stevenson, 1989; Pappalardo et al., 1999), that is supposed to contribute to the formation of the intrinsic magnetic field of Ganymede, induced by the presence of conducting fluid and salty layer (Kivelson, Khurana, & Volwerk, 2002; Sarson, Jones, Zhang, & Schubert, 1997; Schubert et al., 2004; Sohl et al., 2002). The magnetic field of this satellite may also relate to a dynamo mechanism in the metallic core (Schubert, Zhang, Kivelson, & Anderson, 1996).

The surface of Ganymede is subdivided into two main terrains (Figure 1). These are the dark and the light terrains (Collins et al., 2013; Patterson et al., 2010; Shoemaker, Lucchitta, Wilhelms, Plescia, & Squyres, 1982; Smith et al., 1979b) and show distinct surface characteristics including different albedo, crater density and morphotectonic structures (Bianchi, Casacchia, Lanciano, Pozio, & Strom, 1986; Collins et al., 2013; Lucchitta, 1980; Murchie, Head, & Plescia, 1990; Parmentier, Squyres, Head, & Allison, 1982; Patterson et al., 2010; Prockter et al., 1998, 2000). The dark terrain covers 35% of the surface and it is characterized by relatively low albedo material (0.26 ± 0.05 according to Helfenstein et al., 1997) and high crater density, whose measurement suggests an age of around 4 Gyr (Nimmo & Pappalardo, 2004; Zahnle, Dones, & Levison, 1998, 2003). They are characterized by large-scale, arcuate fracture systems termed furrows, that have been hypothesized to be impact-related as the remnants of a system of concentric rings and radial fractures produced by large impacts occurred in the early

**CONTACT** Costanza Rossi costanza.rossi@uniroma3.it GeoQuTe Lab, Science Department, Roma Tre University, L.go S. L. Murialdo 1, I-00146, Rome, Italy

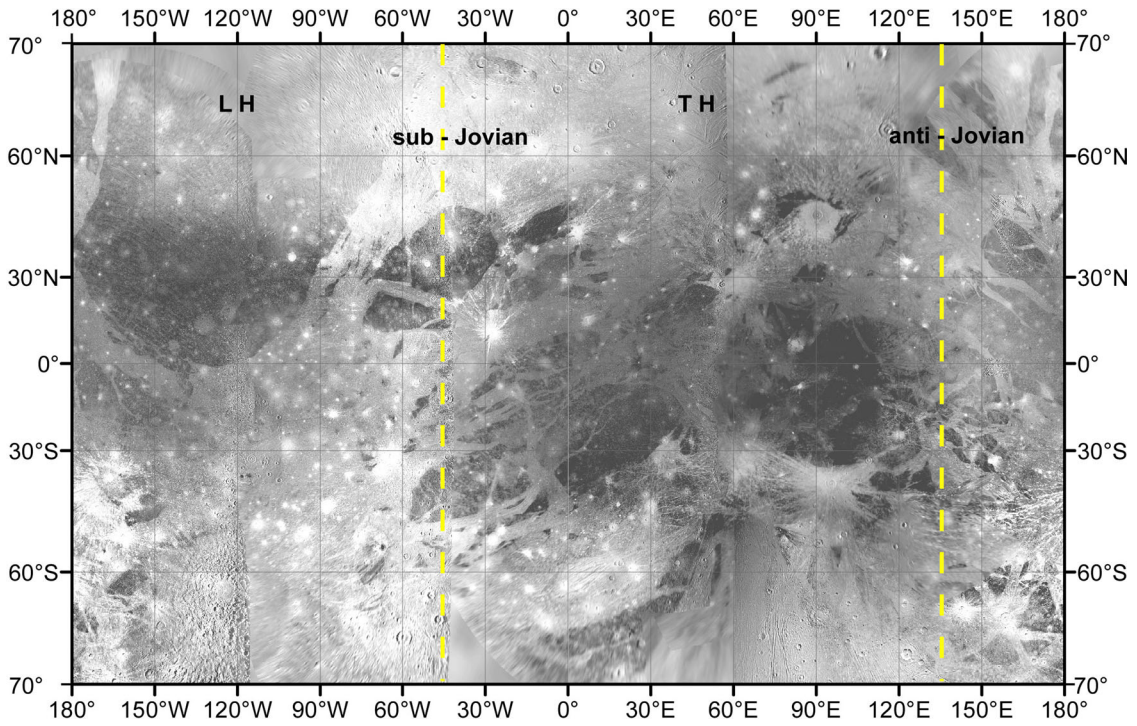


**Figure 1.** Ganymede Voyager and Galileo Global Mosaic, Mercator projection. The dashed yellow lines define the boundaries of the leading (LH in figure) and the trailing (TH) hemispheres at the W and E, respectively.

history of Ganymede, when its icy crust was thinner (Casacchia & Strom, 1984; McKinnon & Melosh, 1980; Murchie et al., 1990 Prockter et al., 1998; Schenk & McKinnon, 1987;). Furrows are mainly cut by younger landforms, craters, and by the light terrain regions. The dark terrain shows local areas, the lineated units according to Patterson et al. (2010) and Collins et al. (2013), where linear fractures lie in between the dark and the light terrains. These units represent possible key areas to understand the relation and transition between the two terrains (Prockter, Figueredo, Pappalardo, Head, & Collins, 2000; Rossi, Cianfarra, Salvini, Mitri, & Massé, 2018).

The other 65% of the satellite surface is covered by the light terrain and is characterized by higher albedo (0.42 ± 0.04; Helfenstein et al., 1997). It shows lower crater density that provides a younger age of around 2 Gyr (Nimmo & Pappalardo, 2004; Zahnle, Schenk, Levison, & Dones, 2003). Craters within the light terrain are almost completely obliterated by the presence of numerous morphotectonic lineated landforms, termed grooves (Figure 2). The light grooved terrain of Ganymede (Lucchitta, 1980; Patterson et al., 2010) represents one of the most tectonically disrupted surfaces of the Solar System. The high density of morphotectonic structures within the light terrain, together with the lower crater counting, confirms the more recent activity of this terrain. A map of the Ganymede grooves has been proposed by Collins, Head, Pappalardo, and Team (2000).

In this work, we investigate and map the pattern of Ganymede regional grooves with the preparation of a structural map for a better comprehension of their characteristics and relationships. Results show that groove structures behave as regional swarms/systems with their own characteristics and structural meaning. In this way, the proposed map considers the sets of regional grooves and shows their regional, organized clustering into systems.

The map represents a base that can be used to investigate the tectonic mechanisms affecting the satellite light terrain as well as to clarify the operating geodynamic processes. We unravel the most recently active regions of Ganymede that are the light terrain deformed by grooves. The main differences between grooves and furrows are age, spacing, morphology, and supposedly origin (Patterson et al., 2010; Rossi et al., 2018). The furrow impact origin took place before the period of grooved terrain formation, as evidenced by the abrupt transection relationships of the two terrains (McKinnon & Melosh, 1980). Due to their external cause, furrows were ignored in the preparation of the final map and their investigation is

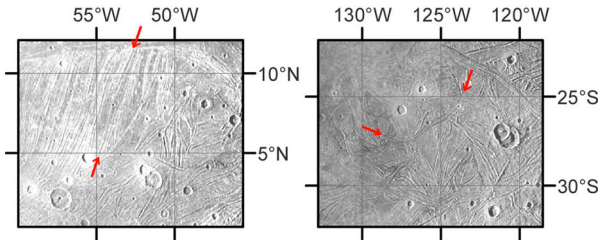


**Figure 2.** Grooved terrain. The red arrows show groove examples.

beyond the goals of the presented structural map that focuses on the more recent tectonic processes and on the internal geodynamic factors ruling the present-day groove characteristics and geometries.

Grooves play a key role in the possible connection between surface and the subsurface ocean and represent the evidence of tectonic activity that deformed the satellite surface during its geologic evolution.

### 1.1. Grooves of Ganymede

Grooves are common, rather linear, structural elongated landforms occurring on the surface of several small bodies of the Solar System as Phobos, Phoebe, Gaspra, Ida, Eros (Morrison, Thomas, Tiscareno, Burns, & Veverka, 2009; Watters & Schultz, 2010). Their morphology varies from linear surface depressions to curvilinear and/or rows of coalesced pits, with lengths spanning from 5 km to over 50 km. Typically they are 100–200 km long and nearly less than 100 m deep (Watters & Schultz, 2010). It is assumed that grooves of the mentioned bodies are subsurface fractures likely produced from extensional tectonic processes (Prockter et al., 2002; Thomas, 1989; Watters & Schultz, 2010). It is generally assumed that grooves are associated with internally-driven tectonics on larger satellites such as Europa, Ganymede, Enceladus, Tethys, and Mimas (Morrison et al., 2009; Pappalardo, 2006; Watters & Schultz, 2010).

Planetary-wide grooved terrains have been firstly observed on the Ganymede surface (Lucchitta, 1980; Shoemaker et al., 1982). Grooves of Ganymede (Figure 2) represent the brittle deformation of the light terrain of the satellite. They occur, as observed at the regional scale, clustered into sets of grooves with length > 100 km and average spacing of about 10 km (Bianchi, Casacchia, & Pozio, 1984; Casacchia & Strom, 1984; Collins et al., 2000, 2013; Lucchitta, 1980; Pappalardo et al., 1998, 2004; Pappalardo & Greeley, 1995; Patterson et al., 2010). They often cluster in nearly parallel ordered patterns.

The stress fields and the tectonic processes that generate grooves remain still unclear. Authors (e.g. Bland & Showman, 2007; Collins, Head, & Pappalardo, 1998; Lucchitta, 1980; Pappalardo et al., 1998; Parmentier, 1982; Philpott, 1988; Pizzi et al., 2017; Shoemaker et al., 1982; Squyres & Croft, 1986) interpret the global assemblage of Ganymede grooves as extensional zones similar to the Earth continental rifts, resulting from the global expansion that affected the satellite crust in the past. In addition to normal faulting, strike-slip motion was observed within small regions of grooved terrain (Cameron et al., 2018; Collins et al., 1998; Lucchitta, 1980; Murchie & Head, 1988; Pappalardo et al., 1998; Pappalardo & Collins, 2005). More recently, a regional scale shear component is suggested to play a key role in the evolution of large grooved terrain regions (Cameron et al., 2018; Rossi et al., 2018; Seifert, Cameron, Smith-Konter, Pappalardo, & Collins, 2015). Several regions imaged by the Galileo spacecraft were investigated applying structural geological methodologies. *Dardanus Sulcus* is centred at 17.5° S, 342.5° E and both extension and right-lateral strike-slip tectonics originated its grooves (Cameron, Smith-Konter, Burkhard, Pappalardo, & Collins, 2016; 2018; Cameron, Smith-Konter, Pappalardo, Collins, & Nimmo, 2013; Seifert et al., 2015). *Arbela Sulcus* (21.1° S, 10.2° E) was formed, similarly to *Dardanus Sulcus*, by an extension event dissecting the upper crust (Berquin, Kofman, Herique, Alberti, & Beck, 2013; Giese, Wagner, Neukum, Pappalardo, & Head, 2001; Head et al., 2002) with a left-lateral shear component (Cameron et al., 2018; Head et al., 2002). Events of tectonic deformation suggesting extensional and strike-slip regimes were proposed also for *Nun Sulci* grooves (49.5° N, 43.6° E; Cameron et al., 2018; Murchie & Head, 1988; Seifert et al., 2015), *Nippur/Philus Sulcus* (36.9° N, 175° E), *Byblus Sulcus* (37.9° N, 160.1° E) and *Anshar Sulcus* (18°N, 162.1° E) (Cameron et al., 2018 and references therein). *Tiamat Sulcus* (3.4° N, 151.5° E) and *Kishar Sulcus* (6.4° S, 216.6° W) represent a labyrinth of intersecting grooves suggesting strike-slip shear (Bedle & Jurdy, 2005; Cameron et al., 2016; 2018; Murchie & Head, 1988) as well as in *Harpagia Sulcus* (11.8° S, 313.5° W; Berquin et al., 2013; Head et al., 2002). *Uruk Sulcus* is a broadly studied light terrain of Ganymede. Studies on a target site of this sulcus (0.8° N; 199.7° E) imaged within the sulcus at high-resolution by Galileo probe infer extension with normal faulting, graben and domino-style mechanisms (Pappalardo et al., 1998). These Authors recognized also local transtensional shear within it. More recent investigations based on the Voyager imagery of *Uruk Sulcus* at regional scale allowed to recognize the consistent role of transpressional strike-slip kinematics along the region with significant compressional component (Rossi et al., 2018).

Despite these numerous studies, the regional geological setting of most grooved terrain is still poorly known. In this way, a map of classified Ganymede grooves represents a tool to improve the knowledge on the tectonic evolution of the satellite. The map highlights the spatial organization of these features, i.e. their spatial distribution, crosscutting relationship, and azimuthal clustering. This mapping represents a tool to recognize the spatial distribution of these properties. Manually detected grooves of Ganymede were quantitatively classified into regional systems by a structural geology approach. This map represents the tool to further investigate the stress conditions associated to the groove formation and evolution. This information is relevant to the preparation of future space missions.

## 2. Data

Ganymede imagery derives from planetary missions across the Outer Solar System. The high-resolution images used in this work belong to the Wide Angle Camera (WAC) and Narrow Angle Camera (NAC) onboard the twin Voyager 1 and 2, and the Galileo Solid State Imaging (SSI) camera that largely covered the satellite (a full set of these image data is available on http://pds.jpl.gov).

The mapping was based on the remote sensing investigation of a monochrome base map of the satellite released by the United States Geological Survey (USGS) Astrogeology Science Centre (available on http://astrogeology.usgs.gov). This is the Ganymede Voyager and Galileo Global Mosaic, a Mercator projected map derived from the mosaicking of the best image quality and resolution coverage (from 20 km/pixel for gap fill to approximately 400 meters/pixel) supplied by NAC and SSI cameras (Figure 1; Becker et al., 2001). Most of the best data of Voyager and Galileo were obtained within the leading hemisphere of Ganymede (Figure 1).

## 3. Structural mapping

Regional grooves of Ganymede were mapped between 60°N and 60°S and digitized in a geographic information system (GIS) geodatabase.

Image with low-resolution and high geometric distortion in some areas of the satellite prevented their use for mapping purposes. For this reason, grooves were mapped on approximately 36% of the light terrain (as mentioned, about 50% of the light terrain images were not acceptable for manual mapping). The polar regions were excluded in this work due to the distortion limits of most of the available images for these.

A total of 14,707 groove structures have been recognized and digitized between 60°N and 60°S (Figure 3). A lack of data occurs in the region included within 60° E and 80°E due to the low-resolution of the available images (resolution lower than 2000 m/pixel). This zone partly falls of the anti-Jovian hemisphere of Ganymede.

Mapped grooves are considered as the topographic expression of trough structures. Their bottom is recognized thanks to the luminosity contrast resulting from the solar lighting conditions. Grooves with higher tonal intensity were digitized as polylines. These were quantitatively analysed according to the azimuth of their segments. Statistical analyses of the identified grooves allow to classify the majority of these structures into clusters of azimuthal families.

### 3.1. Azimuthal Analysis

The grouping of the families of grooves into regional systems is based on their azimuths and spatial distribution. Each groove is represented as a georeferenced series of contiguous segments (a total of 50,717 segments forming 14,707 polylines) characterized by their azimuths and lengths. The preliminary azimuthal frequency analysis of the total segments is presented in Figure 4. This process includes the polymodal analysis by best fit of the frequency histogram with a function sum of Gaussian curves (Daisy

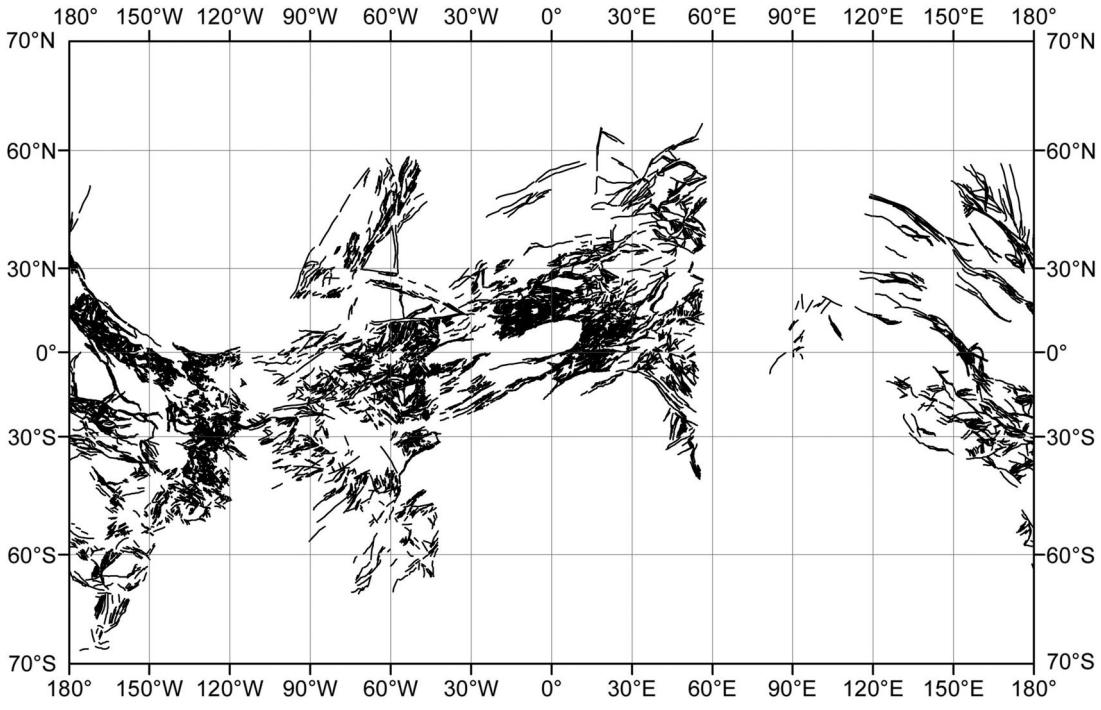


Figure 3. Grooves global mapping, Mercator projection. A total of 14,707 identified regional grooves is shown.

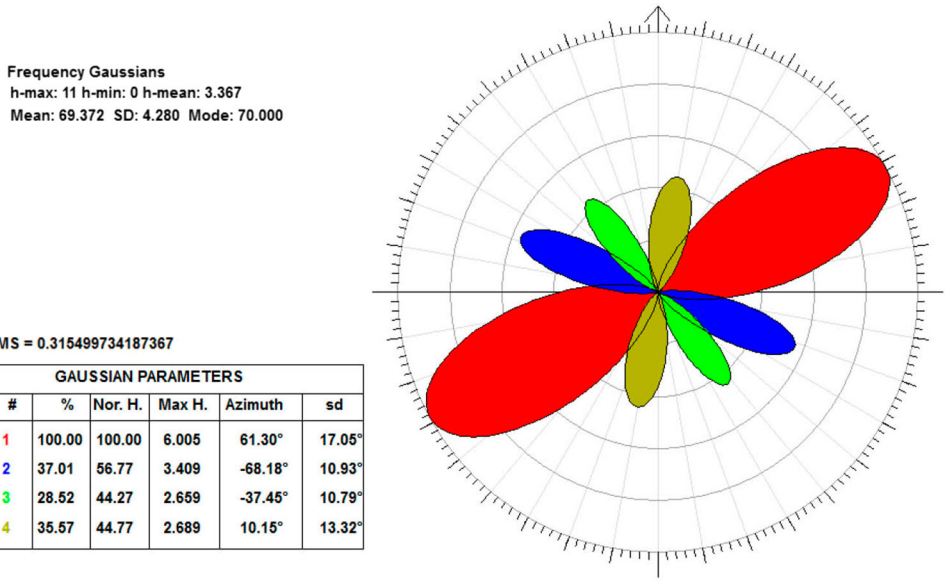


GAUSSIAN PARAMETERS

| # | % | Nor. H. | Max H. | Azimuth | sd |
|---|---|---|---|---|---|
| 1 | 100.00 | 100.00 | 6.005 | 61.30° | 17.05° |
| 2 | 37.01 | 56.77 | 3.409 | -68.18° | 10.93° |
| 3 | 28.52 | 44.27 | 2.659 | -37.45° | 10.79° |
| 4 | 35.57 | 44.77 | 2.689 | 10.15° | 13.32° |

**Figure 4.** Cumulative azimuthal analysis of the mapped grooves. The Gaussian Parameter are reported in the lower left table: the number of Gaussian peaks (#), the percentage of occurrence (%), the Normalized Height (NorH), the Maximum height (MaxH), the azimuth, and the standard deviation (sd). The preferential Gaussian peaks represent the azimuthal interval for the classification into super-systems.

version 5.36.71; Salvini, 2019). This allows to recognize the presence of multiple preferred orientations (i.e. relative maxima in the histograms) and to characterize each azimuthal cluster with its statistical parameters: mean azimuth, standard deviation, and relative height (Cianfarra & Salvini, 2016a; Wise, Funiciello, Parotto, & Salvini, 1985). Results show that groove segments cluster into 4 preferred orientations, namely: N61°E, N68°W, N37°W, and N10°E (Figure 4). Considering the rotation produced by the almost spherical geometry of Ganymede surface and to follow possible regional rotations within each group, the grooves classification was performed by the comparison of their azimuths within a spatial grid of circular areas. The grid resolution pace was 20° of latitude and longitude in a hexagonal shape. A diameter of 6000 km was chosen for each circular area to guarantee the partial overlap between adjacent circular analyses and to ease the detection of continuity among the analyses (Figure 5). The specific approach we used in searching for groove swarms accomplishes for swarm rotations due to both the spherical shape of the surface and possible swarm rotation across the regions. This has been obtained by comparing the found Gaussian peak among the results of adjacent analyses. This procedure automatically takes care of both distortion/rotation.

A total of 148 circles form the grid. For each circle the azimuthal frequency analysis of the segments of the internally falling grooves was performed to identify the preferred orientations within the considered circle. Azimuthal groups are presented in Figure 5 in the form of oriented lines (i.e. Gaussian peaks) proportional to the relative importance in wind-rose diagrams centred at the grid nodes. These Gaussian peaks were then grouped by comparing their mean azimuth with the Gaussians of the surrounding analyses. Among the unclassified Gaussians (obviously all of them in the first cycle) the largest Gaussian is identified by their relative height and the corresponding number of segments and it becomes the seed of the system to be identified. Then its azimuth is compared with the azimuths of the Gaussians in the 6 surrounding analyses. In each of them, the Gaussian with the closest mean azimuth and having an angle to the seed smaller than a given reference value (5° for this analysis) is classified as belonging to the searched system. Then each newly classified Gaussian becomes a seed for the search of the system and the process is repeated in a recursive way (forest-fire process, Turcotte, 1997) until no contiguous analyses have Gaussians associable to the system (i.e. all the remaining unclassified Gaussians forming angles larger than the reference one) or all the analyses have been inspected. This process is repeated by identifying a new seed Gaussian to search for other systems until all Gaussians have been classified (Figure 5). Spatial rotation of grooves systems is guaranteed by the tolerance of rotations between adjacent peaks to pertain to the same system (5°/6000 km in this study). The result of this analysis brought to the identification of 23 systems, formed within the 361 found Gaussians and is presented in Figure 6 where the systems are colour coded. The further azimuthal analyses of found Gaussians allow to group the found systems to form 4 super-systems, with azimuthal intervals: the NE super-system N61°E ± 17°, the WNW super-system N68°W ± 11°, the NW super-system N37°W ± 11°,

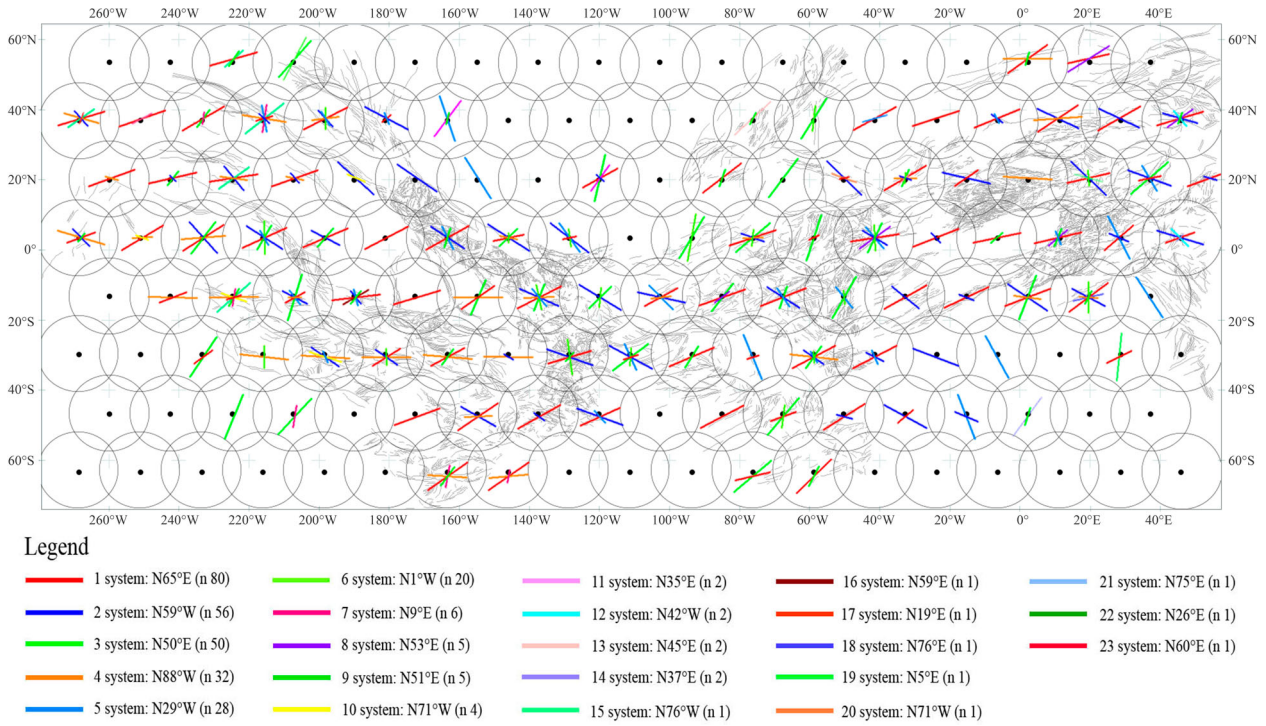


**Figure 5.** Azimuthal grid analysis, Equidistant Cylindrical projection. Circles of the grid are represented as their mean dimension at the equator. In the circle centres are shown the classified Gaussians; in background the mapped grooves are represented. The legend explains the mean azimuth and the peak number (*n*) of each system of the grid analysis.

and the N-S super-system N10°E ± 13°. Segments are then associated with the found systems in a similar procedure. Their azimuths are compared to the Gaussians from the analysis of the circular areas where the groove falls, and it is associated to the system having the smallest angle to the corresponding Gaussian mean azimuth and lower than a reference minimum (20° in this study). When the last requirement is not satisfied, the segment is associated to the null (0) system and remains unclassified. As a result, Grooves are associated to super-systems by associating to each groove the system that is best represented within its segments.

## 4. Groove super-systems

A total of 14,707 grooves (i.e. polylines) were analysed and are shown in the Main Map. The classified structures represent super-systems, groups of grooves that locally crosscut and intersect each other, and are globally arranged according to azimuthal/spatial clustering. At the regional scale they cluster to form 4 super-systems, distributed all over the investigated surface. Strong evidence of clear crosscutting relationships is difficult to identify among the found super-systems. Conversely, several local areas show a recognizable chronological sequence. The classification allows to

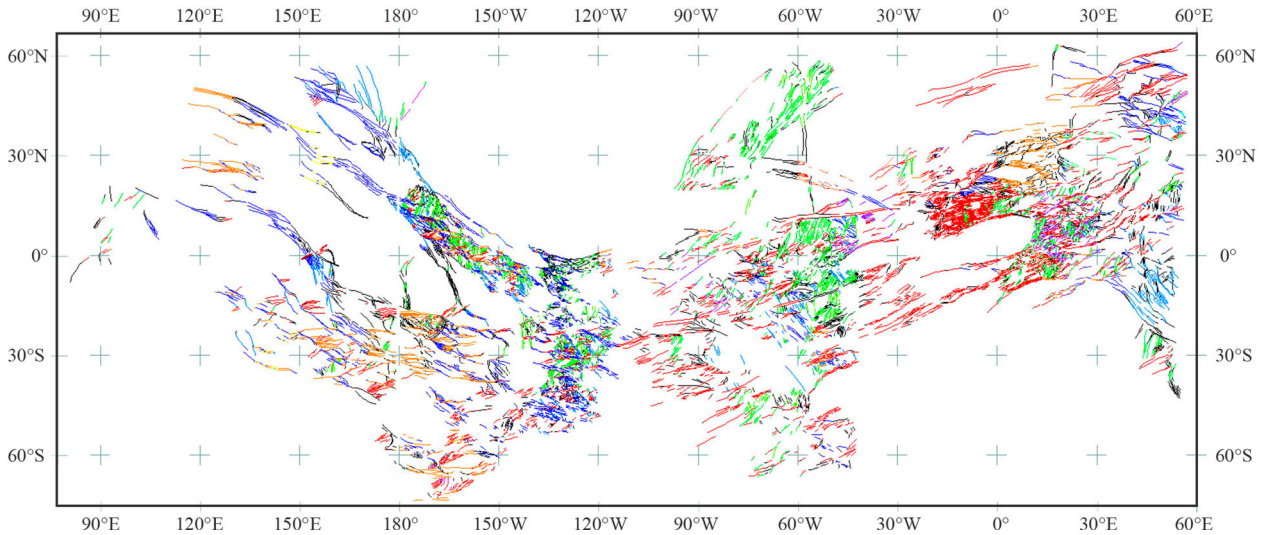


**Figure 6.** Identification of the 23 main systems associated to super-systems shown in Figure 4. Colour-coded legend is reported in Figure 5; black lines represent unclassified groove elements.

identify a total of 4 super-systems, composed by 11,402 grooves, and leaved unclassified 3305 ones.

The largest super-system is the NE super-system (3992 grooves). It is represented in red colour in the Main Map and shows a mean direction of N61°E. Its spatial density is higher between approximately 120° W and 50°E, where it presents the longer grooves. This region corresponds to *Babylon Sulci* and *Phrygia Sulcus*, where grooves of this super-system mainly cut the other ones.

The second super-system is the WNW super-system (2898 grooves). It is represented in blue colour in the Main Map and shows a mean direction of N68°W. It mainly occurs between 120°E and 120° W, corresponding to *Tiamat Sulcus*, *Kishar Sulcus*, *Lagash Sulcus*, *Anshar Sulcus*, *Mashu Sulcus*, *Byblus Sulcus*, *Uruk Sulcus*, and *Nippur Sulcus*. In these regions, it presents the longer groove elements that mostly cut the other. Between 130°W and 120°W this super-system coexists with the NE one, and it is characterized by the similar crosscutting relationships of the NE super-system.

The third super-system is the NW one (1182 grooves). It is represented with light blue colour in the Main Map and shows a mean direction of N37° W. It is mainly spatially distributed where the WNW super-system occurs. In this way, it is mostly present between 150°E and 120°W, groove clusters from this super-system are also present between 70°W and 50° W, and 45°E–60°E, where they are cut by the grooves of the NE super-system.

The fourth super-system is the N-S (3330 grooves). It is represented with yellow colours in the Main Map and shows a mean direction of N10°E. It mostly clusters between 90°W and 40°W, where it is mainly cut by the first super-system. Conversely, within 180° and 120°W it is mainly cut by the WNW super-system. Grooves from this super-system as well as from the NW one are notably shorter than the grooves of the other super-systems (groove mean length is about 90 km).

The unclassified grooves (3305 grooves, in black colour in the Main Map) present an un-clustered organization and are evenly distributed on Ganymede light terrain.

## 5. Discussion

Grooves of Ganymede group into organized azimuthal families with small internal rotation through the Ganymede surface. The performed classification allows to recognize groove azimuthal super-systems developed at the global scale. Specific main orientations were identified and reflect the tectonic setting of the regions where they develop across the satellite surface. The chronological succession is difficult to be unravelled at the regional scale, and it was not possible to recognize a definitive relative chronological sequence of the found super-systems.

The global geologic map of Ganymede (Collins et al., 2013) determined the relative age relationships among the recognized units based on cross-cutting relationships and divided the light material units into three relative age categories.

The comparison of the found super-systems with these units and their proposed relative age (Collins, 2009; Collins et al., 2013; Patterson et al., 2010) allows to roughly recognize a relative time sequence of the found super-systems. By taking into account that this comparison is between groove structures and terrains, we can assume that the NE and the WNW super-systems mostly occur in the youngest light material units; the NW and the N-S super-systems mostly occur within the intermediate units. The oldest units mainly correspond to the location of the N-S super-system.

On the other hand, the super-system spatial organization provides information about the tectonics that caused them. The super-system framework distinguishes provinces that are characterized by different stress regimes. Grooves of super-systems are often distributed following recognizable geometries. The presence of longer and parallel grooves that bound areas with shorter grooves is common. These longer elements seem likely to act as main shear boundaries that confine elongated region of deformation characterized by the presence of shorter and closer elements. This resembles regional corridors on the Earth surface (Cianfarra & Maggi, 2017; Cianfarra & Salvini, 2014, 2015, 2016b; Maggi, Cianfarra, & Salvini, 2016; Pinheiro, Cianfarra, Villela, & Salvini, 2019; Storti, Holdsworth, & Salvini, 2003;). Several areas of Ganymede light terrain follow a similar corridor geometry associated to strike-slip kinematics. At the regional scale, Authors (e.g. Rossi et al., 2018) recognized this setting within *Uruk Sulcus* area that is suggested to be a strike-slip corridor. *Babylon Sulci* also may represent a similar example of this strike-slip setting (from 70°W to 30° W). There the NE super-system delineates longer and sub-parallel grooves that enclose shorter grooves with different directions. Other examples produced by the NE super-system are found within *Phrygia Sulcus*. This confirms the key role that the strike-slip tectonic regime plays at the regional scale, as already observed at the local one (Bedle & Jurdy, 2005; Berquin et al., 2013; Cameron et al., 2018; Giese et al., 2001; Head et al., 2002; Murchie & Head, 1988; Pappalardo et al., 1998; Seifert et al., 2015). Often the transition between the dark and the light terrains is characterized by the presence of isolated grooves of the super-systems (mainly the NE and the WNW one). Their length and well-defined evidence suggest a kinematic origin. This strengthens the importance of horizontal displacement between the terrains.

The Main Map reports two distinct regions where the NE and the WNW super-systems prevail. The NE super-system mainly occupies the so-called trailing hemisphere of the satellite, and the WNW one mostly develops in the leading hemisphere (Figure 1). The NE and the WNW super-systems systematically cut the other super-systems. Their activity may partially relate to the tidal process that influences the spatial arrangement of the NE and WNW super-systems. The sub- and anti-Jovian hemispheres show a similar distinction (Figure 1). It is observed a prevalence of the NE super-system within the sub-Jovian hemisphere, and a prevalence of the WNW super-system within the anti-Jovian one.

Part of the anti-Jovian hemisphere of Ganymede lack significative information due to the low resolution of the available imagery. This precludes interpretation regarding the effects of tidal process in the anti-Jovian hemisphere.

It is possible that tidal heating coexisted together with other geodynamic processes as convection (e.g. Hammond & Barr, 2014), near-surface partial melt (e.g. Bland, Showman, & Tobie, 2009), and/or polar wandering (e.g. Matsuyama, Nimmo, & Mitrovica, 2014; Mohit, Greenhagen, & McKinnon, 2004; Murchie & Head, 1986).

This map represents the base for future structural researches and exploration of the satellite. The distribution and characteristics of mapped grooves are strictly related to anisotropy of the terrain (both crustal thickness and rheology/composition) that will be significant for the programmed radar instrumentation (e.g. Radar for Europa Assessment and Sounding: Ocean to Near-surface, REASON, Pettinelli et al., 2015; Radar for Icy Moon Exploration, RIME, Bruzzone et al., 2013). The identified groove azimuths will be useful to identify regions where to acquire the optimal data and to avoid intense clutter returns (Ilyushin, Orosei, Witasse, & Sánchez-Cano, 2017).

## 6. Conclusions

The presented structural map of Ganymede regional groove systems shows the spatial arrangement of the regional grooves into super-systems. They represent the effect of the tectonics on the satellite and their mapping identifies distinct geometries that provide information on the tectonic setting. The map derives from a systematic investigation and represents an important tool to study groove pattern and clustering.

A total of 14,707 grooves were identified and reported on the map. Azimuthal analysis allowed to classify a total of 11,402 (77.5%) grooves into 4 super-systems regionally distributed, that show an arrangement similar to the strike-slip corridors of the Earth. This classification leaves unclassified 3305 (22.5%) scattered grooves.

The two main super-systems, namely the NE and WNW ones, preferentially occupy the leading and the trailing hemispheres, respectively. Tidal deformation may be responsible for the symmetrical pattern of these super-systems.

This map is a useful tool for future more detailed structural analyses to investigate the groove spatial distribution, the processes that led to their formation, and their possible fractal distribution (Lucchetti, Pozzobon, Mazzarini, Cremonese, & Massironi, 2017).

The used statistical approach represents an effective method to classify stress-related structures. It may contribute and provide potential support to study the geodynamic processes of the satellite.

Future missions that will provide a better quality of image coverage, allow to complete the mapping also of the polar regions and the low-resolution quadrant of the anti-Jovian hemisphere. This map improves the knowledge of the surface environment for the future exploration of Ganymede.

## Software

The structural map of Ganymede regional groove systems was prepared by using the QGIS software. Azimuthal analyses were performed by using the DAISY3 software developed by F. Salvini and freely distributed at: http://host.uniroma3.it/progetti/fralab.

## Acknowledgements

We kindly acknowledge Makram Murad-al-shaikh, Yaroslaw A. Ilyushin and Geoffrey Collins for the insightful comments that allowed to improve the manuscript and the map. Thanks to Federico Galetto for the assistance and useful comments. Funding for this project came from Roma Tre University (fellowship) and the Roma Tre GeoQuTe lab, project RP-03. This work has been completed within the PhD project of the first author.

## Disclosure statement

No potential conflict of interest was reported by the authors.

## Funding

This work was supported by the Università degli Studi Roma Tre [PhD fellowship].

## References

Anderson, J. D., Jacobson, R. A., Lau, E. L., Moore, W. B., Olsen, O., Schubert, G., & Thomas, P. C. (2001). Shape, mean radius, gravity field and interior structure of Ganymede. *Bulletin of the American Astronomical Society*, *33*, 1101.

Anderson, J. D., Lau, E. L., Sjogren, W. L., Schubert, G., & Moore, W. B. (1996). Gravitational constraints on the internal structure of Ganymede. *Nature*, *384*(6609), 541–543. doi:10.1038/384541a0

Becker, T., Archinal, B., Colvin, T., Davies, M., Gitlin, A., Kirk, R. L., & Weller, L. (2001). Final digital global maps of Ganymede, Europa, and Callisto. *Lunar and Planetary Science Conference*, 32.

Bedle, H., & Jurdy, D. M. (2005). Ganymede's sulci on global and regional scales. *Lunar and Planetary Science*, *XXXVI*, 1161.

Berquin, Y., Kofman, W., Herique, A., Alberti, G., & Beck, P. (2013). A study on Ganymede's surface topography: Perspectives for radar sounding. *Planetary and Space Science*, *77*, 40–44. doi:10.1016/j.pss.2012.07.004

Bianchi, R., Casacchia, R., Lanciano, P., Pozio, S., & Strom, R. G. (1986). Tectonic framework of grooved terrain on Ganymede. *Icarus*, *67*(2), 237–250. doi:10.1016/0019-1035(86)90106-5

Bianchi, R., Casacchia, R., & Pozio, S. (1984). Tectonics of the grooved terrain on Ganymede. *Lunar and Planetary Science Conference*, *15*, 54–55.

Bland, M. T., & Showman, A. P. (2007). The formation of Ganymede's grooved terrain: Numerical modeling of extensional necking instabilities. *Icarus*, *189*(2), 439–456. doi:10.1016/j.icarus.2007.01.012

Bland, M. T., Showman, A. P., & Tobie, G. (2009). The orbital–thermal evolution and global expansion of Ganymede. *Icarus*, *200*(1), 207–221. doi:10.1016/j.icarus.2008.11.016

Bruzzone, L., Plaut, J. J., Alberti, G., Blankenship, D. D., Bovolo, F., Campbell, B. A., … Seu, R. (2013). RIME: Radar for icy moon exploration. *2013 IEEE International geoscience and remote sensing symposium-IGARSS*, 3907–3910.

Cameron, M. E., Smith-Konter, B. R., Burkhard, L., Collins, G. C., Seifert, F., & Pappalardo, R. T. (2018). Morphological mapping of Ganymede: Investigating the role of strike-slip tectonics in the evolution of terrain types. *Icarus*, *315*, 92–114. doi:10.1016/j.icarus.2018.06.024

Cameron, M. E., Smith-Konter, B. R., Burkhard, L., Pappalardo, R. T., & Collins, G. C. (2016). Strike-slip faulting on Ganymede: morphological mapping and failure mechanics. *Lunar and Planetary Science Conference*, *47*, p. 2630.

Cameron, M. E., Smith-Konter, B. R., Pappalardo, R. T., Collins, G., & Nimmo, F. (2013). Tidally-driven strike-slip failure mechanics on Ganymede. *Lunar and Planetary Science Conference*. Technical Report 44. Lunar and Planetary Institute, p. 2711.

Carr, M. H., Belton, M. J. S., Chapman, C. R., Davies, M. E., Geissler, P., Greenberg, R., … Veverka, J. (1998). Evidence for a subsurface ocean on Europa. *Nature*, *391*(6665), 363–365.

Casacchia, R., & Strom, R. G. (1984). Geologic evolution of Galileo Regio, Ganymede. *Journal of Geophysical Research: Solid Earth*, *89*, S02. doi:10.1029/JB089iS02p0B419

Cianfarra, P., & Maggi, M. (2017). Cenozoic extension along the reactivated Aurora Fault System in the East Antarctic Craton. *Tectonophysics*, *703*, 135–143. doi:10.1016/j.tecto.2017.02.019

Cianfarra, P., & Salvini, F. (2014). Ice sheet surface lineaments as nonconventional indicators of East Antarctica bedrock tectonics. *Geosphere*, *10*(6), 1411–1418. doi:10.1130/GES01074.1

Cianfarra, P., & Salvini, F. (2015). Lineament domain of regional strike-slip corridor: Insight from the Neogene transtensional De Geer transform fault in NW Spitsbergen. *Pure Applied Geophysics*, *172*(5), 1185–1201. doi:10.1007/s00024-014-0869-9

Cianfarra, P., & Salvini, F. (2016a). Quantification of fracturing within fault damage zones affecting late Proterozoic carbonates in Svalbard. *Rendiconti Lincei*, *27*(1), 229–241. doi:10.1007/s12210-016-0527-5

Cianfarra, P., & Salvini, F. (2016b). Origin of the adventure subglacial trench linked to Cenozoic extension in the East Antarctic Craton. *Tectonophysics*, *670*, 30–37. doi:10.1016/j.tecto.2015.12.011

Collins, G. C. (2009). The origin of grooved terrain on Ganymede. *European Planetary Science Congress*, *4*, 516.

Collins, G. C., Head III, J. W., & Pappalardo, R. T. (1998). The role of extensional instability in creating Ganymede grooved terrain: Insights from Galileo high-resolution stereo imaging. *Geophysical Research Letters*, *25*(3), 233–236. doi:10.1029/97GL03772

Collins, G. C., Head, J. W., Pappalardo, R. T., & Team, G. S. (2000). A global database of grooves and dark terrain on Ganymede, enabling quantitative assessment of terrain features. *Lunar and Planetary Science Conference*, p. 31.

Collins, G. C., Patterson, G. W., Head, J. W., Prockter, L., Pappalardo, R. T., Lucchitta, B. K., & Kay, J. P. (2013). Global geologic map of Ganymede. US Department of the Interior, US Geological Survey. doi:10.3133/sim3237.

Deschamps, F., & Sotin, C. (2001). Thermal convection in the outer shell of large icy satellites. *Journal of Geophysical Research: Planets*, *106*(E3), 5107–5121. doi:10.1029/2000JE001253

Fanale, F. P., Johnson, T. V., & Matson, D. L. (1977). Io's surface and the histories of the Galilean satellites. *IAU Colloq. 28: Planetary Satellites*, pp. 379–405.

Fimmel, R. O., Van Allen, J., & Burgess, E. (1980). Pioneer: first to Jupiter, Saturn, and beyond. NASA Special Publication 446.

Giese, B., Wagner, R., Neukum, G., Pappalardo, R. T., Head, J. W., & the Galileo SSI Team (2001). The topography of Ganymede's Arbela Sulcus. *Lunar and Planetary Science*, *XXXII*, 1743.

Grasset, O., Dougherty, M. K., Coustenis, A., Bunce, E. J., Erd, C., Titov, D., … Van Hoolst, T. (2013). Jupiter icy moons Explorer (JUICE): An ESA mission to orbit Ganymede and to characterise the Jupiter system. *Planetary and Space Science*, *78*, 1–21. doi:10.1016/j.pss.2012.12.002

Hammond, N. P., & Barr, A. C. (2014). Formation of Ganymede's grooved terrain by convection-driven resurfacing. *Icarus*, *227*, 206–209. doi:10.1016/j.icarus.2013.08.024

Head, J. W., Pappalardo, R. T., Collins, G. C., Belton, M. J. S., Giese, B., Wagner, R., … Moore, J. (2002). Evidence for Europa-like tectonic resurfacing styles on Ganymede. *Geophysical Research Letters*, *29*(24), 2151. doi:10.1029/2002GL015961

Helfenstein, P., Veverka, J., Denk, T., Neukum, G., Head, J. W., Pappalardo, R. T., & the Galileo Imaging Team. (1997). Dark-floor craters: Galileo constraints on a Ganymede regolith component. *Lunar and Planetary Science*, *XXVIII*, 547–548.

Hussmann, H., Sotin, C., & Lunine, J. I. (2007). Interiors and evolution of icy satellites. In T. Spohn & G. Schubert (Eds.), *Treatise on Geophysics. 10* (pp. 509–539). Oxford: Elsevier.

Ilyushin, Y. A., Orosei, R., Witasse, O., & Sánchez-Cano, B. (2017). CLUSIM: A synthetic aperture radar clutter simulator for planetary exploration. *Radio Science*, *52*(9), 1200–1213.

Khurana, K. K., Kivelson, M. G., Stevenson, D. J., Schubert, G., Russell, C. T., Walker, R. J., & Polanskey, C. (1998).

Induced magnetic fields as evidence for subsurface oceans in Europa and Callisto. *Nature*, *395*(6704), 777.
Kirk, R. L., & Stevenson, D. J. (1987). Thermal evolution of a differentiated Ganymede and implications for surface features. *Icarus*, *69*(1), 91–134.
Kivelson, M. G., Khurana, K. K., Russell, C. T., Volwerk, M., Walker, R. J., & Zimmer, C. (2000). Galileo magnetometer measurements: A stronger case for a subsurface ocean at Europa. *Science*, *289*(5483), 1340–1343. doi:10.1126/science.289.5483.1340
Kivelson, M. G., Khurana, K. K., & Volwerk, M. (2002). The permanent and inductive magnetic moments of Ganymede. *Icarus*, *157*, 507–522. doi:10.1006/icar.2002.6834
Lucchetti, A., Pozzobon, R., Mazzarini, F., Cremonese, G., & Massironi, M. (2017). Brittle ice shell thickness of Enceladus from fracture distribution analysis. *Icarus*, *297*, 252–264. doi:10.1016/j.icarus.2017.07.009
Lucchitta, B. K. (1980). Grooved terrain on Ganymede. *Icarus*, *44*(2), 481–501. doi:10.1016/0019-1035(80)90039-1
Maggi, M., Cianfarra, P., & Salvini, F. (2016). Erosion by tectonic carving in the Concordia subglacial fault zone, East Antarctica. *Earth and Planetary Science Letters*, *433*, 99–108. doi:10.1016/j.epsl.2015.10.045
Matson, D. L., Spilker, L. J., & Lebreton, J. P. (2003). The Cassini-Huygens mission to the Saturnian system. *The Cassini Huygens Mission*, 1–58. doi:10.1007/978-94-017-3251-2_1
Matsuyama, I., Nimmo, F., & Mitrovica, J. X. (2014). Planetary reorientation. *Annual Review of Earth and Planetary Sciences*, *42*, 605–634. doi:10.1146/annurev-earth-060313-054724
McKinnon, W. B., & Melosh, H. J. (1980). Evolution of planetary lithospheres: Evidence from multiringed structures on Ganymede and Callisto. *Icarus*, *44*(2), 454–471. doi:10.1016/0019-1035(80)90037-8
Mohit, P. S., Greenhagen, B. T., & McKinnon, W. B. (2004). Polar wander on Ganymede. *Bulletin of the American Astronomical Society*, *36*, 1084.
Moore, W. B., & Schubert, G. (1996). New models of Ganymede's internal structure from Galileo observations. *Bulletin of the American Astronomical Society*, *28*, 1139.
Morrison, S. J., Thomas, P. C., Tiscareno, M. S., Burns, J. A., & Veverka, J. (2009). Grooves on small saturnian satellites and other objects: Characteristics and significance. *Icarus*, *204*, 262–270. doi:10.1016/j.icarus.2009.06.003.
Murchie, S., & Head, J. W. (1988). Possible breakup of dark terrain on Ganymede by large-scale shear faulting. *Journal of Geophysical Research*, *93*(B8), 8795–8824. doi:0148-0227/88/007B-4008505.00
Murchie, S. L., & Head, J. W. (1986). Global reorientation and its effect on tectonic patterns on Ganymede. *Geophysical Research Letters*, *13*(4), 345–348.
Murchie, S. L., Head, J. W., & Plescia, J. B. (1990). Tectonic and volcanic evolution of dark terrain and its implications for the internal structure and evolution of Ganymede. *Journal of Geophysical Research: Solid Earth*, *95*(B7), 10743–10768. doi:10.1029/JB095iB07p10743
Nimmo, F., & Pappalardo, R. T. (2004). Furrow flexure and ancient heat flux on Ganymede. *Geophysical Research Letters*, *31*), doi:10.1029/2004GL020763
Ojakangas, G. W., & Stevenson, D. J. (1989). Thermal state of an ice shell on Europa. *Icarus*, *81*(2), 220–241.
Pappalardo, R. T. (2006). Ridge and trough terrains on outer planet satellites. AGU Fall Meeting, 32A-02A2.
Pappalardo, R. T., Belton, M. J. S., Breneman, H. H., Carr, M. H., Chapman, C. R., Collins, G. C., … Williams, K. K. (1999). Does Europa have a subsurface ocean? Evaluation of the geological evidence. *Journal of Geophysical Research: Planets*, *104*(E10), 24015–24055. doi:10.109/1998JE000628
Pappalardo, R. T., & Collins, G. C. (2005). Strained craters on Ganymede. *Journal of Structural Geology*, *27*(5), 827–838. doi:10.1016/j.jsg.2004.11.010
Pappalardo, R. T., Collins, G. C., Head IIIJ. W., Helfenstein, P., McCord, T. B., Moore, J. M., … Spencer, J. R. (2004). Geology of Ganymede. In F. Bagenal, T. Dowling, & W. B. McKinnon (Eds.), *Jupiter - The Planet, satellites, and Magnetosphere* (pp. 363–396). Cambridge, UK: Cambridge University Press.
Pappalardo, R. T., & Greeley, R. (1995). A review of the origins of subparallel ridges and troughs: Generalized morphological predictions from terrestrial models. *Journal of Geophysical Research: Planets*, *100*(E9), 18985–19007.
Pappalardo, R. T., Head, J. W., Collins, G. C., Kirk, R. L., Neukum, G., Oberst, J., … Klaasen, K. (1998). Grooved terrain on Ganymede: First results from Galileo high-resolution imaging. *Icarus*, *135*, 276–302. doi:10.1006/icar.1998.5966
Parmentier, E. M., Squyres, S. W., Head, J. W., & Allison, M. L. (1982). The tectonics of Ganymede. *Nature*, *295*, 290–293.
Patterson, G. W., Collins, G. C., Head, J. W., Pappalardo, R. T., Prockter, L. M., Lucchitta, B. K., & Kay, J. P. (2010). Global geological mapping of Ganymede. *Icarus*, *207*(2), 845–867. doi:10.1016/j.icarus.2009.11.035
Pettinelli, E., Cosciotti, B., Di Paolo, F., Lauro, S. E., Mattei, E., Orosei, R., & Vannaroni, G. (2015). Dielectric properties of Jovian satellite ice analogs for subsurface radar exploration: A review. *Reviews of Geophysics*, *53*(3), 593–641. doi:10.1002/2014RG000463
Philpott, R. (1988). Formation of sulci, grooves and associated stress regimes on Ganymede. *Lunar and Planetary Science Conference*, *19*, 919.
Pinheiro, M. R., Cianfarra, P., Villela, F. N. J., & Salvini, F. (2019). Tectonics of the Northeastern border of the Parana Basin (Southeastern Brazil) revealed by lineaments domain analysis. *Journal of South American Earth Sciences*. doi:10.1016/j.jsames.2019.102231.
Pizzi, A., Di Domenica, A., Komatsu, G., Cofano, A., Mitri, G., & Bruzzone, L. (2017). Spreading vs. rifting as modes of extensional tectonics on the globally expanded Ganymede. *Icarus*, *288*, 148–159. doi:10.1016/j.icarus.2017.01.034
Prieto-Ballesteros, O., Bonales, L. J., & Munoz-Iglesias, V. (2012). Potential habitability of the Jupiter system: Deep aqueous environments in Europa, Ganymede and Callisto. Highlights of Spanish Astrophysics VII, *Proceedings of the X Scientific Meeting of the Spanish Astronomical Society*.
Prockter, L. M., Figueredo, P. H., Pappalardo, R. T., Head, J. W., & Collins, G. C. (2000). Geology and mapping of dark terrain on Ganymede and implications for grooved terrain formation. *Journal of Geophysical Research: Planets*, *105*(E9), 22519–22540. doi:10.1029/1999JE001179
Prockter, L. M., Head, J. W., Pappalardo, R. T., Senske, D. A., Neukum, G., Wagner, R., … Belton, M. J. S. (1998). Dark terrain on Ganymede: Geological mapping and interpretation of Galileo Regio at high resolution. *Icarus*, *135*(1), 317–344. doi:10.1006/icar.1998.5981
Prockter, L. M., Thomas, P., Robinson, M., Joseph, J., Milne, A., Bussey, B., … Cheng, A. (2002). Surface expressions of

structural features on Eros. *Icarus*, *155*, 75–93. doi:10.1006/icar.2001.6770.

Rossi, C., Cianfarra, P., Salvini, F., Mitri, G., Massé, M. (2018). Evidence of transpressional tectonics on the Uruk Sulcus region, Ganymede. Tectonophysics 749, 72–87. doi:10.1016/j.tecto.2018.10.026.

Salvini, F. (2019). Daisy 3: The structural data integrated system analyzer software. University of Roma Tre, Rome. http://host.uniroma3.it/progetti/fralab

Sarson, G. R., Jones, C. A., Zhang, K., & Schubert, G. (1997). Magnetoconvection dynamos and the magnetic fields of Io and Ganymede. *Science*, *276*(5315), 1106–1108. doi:10.1126/science.276.5315.1106

Schenk, P., & McKinnon, W. B. (1987). Ring geometry on Ganymede and Callisto. *Icarus*, *72*(1), 209–234. doi:10.1016/0019-1035(87)90126-6

Schubert, G., Anderson, J. D., Spohn, T., & McKinnon, W. B. (2004). Interior composition, structure and dynamics of the Galilean satellites. In F. Bagenal, T. E. Dowling, & W. B. McKinnon (Eds.), *Jupiter: The planet, satellites and magnetosphere. 1* (pp. 281–306). Cambridge, UK: Cambridge University Press.

Schubert, G., Turcotte, D. L., & Olson, P. (2001). *Mantle convection in the Earth and planets*. Cambridge, UK: Cambridge University Press.

Schubert, G., Zhang, K., Kivelson, M. G., & Anderson, J. D. (1996). The magnetic field and internal structure of Ganymede. *Nature*, *384*(6609), 544–545.

Seifert, F., Cameron, M. E., Smith-Konter, B. R., Pappalardo, R. T., & Collins, G. C. (2015). Global morphological mapping of strike-slip structures on Ganymede. *Lunar and Planetary Science Conference*, 46.

Shoemaker, E. M., Lucchitta, B. K., Wilhelms, D. E., Plescia, J. B., & Squyres, S. W. (1982). The geology of Ganymede. In D. Morrison (Ed.), *Satellites of Jupiter* (pp. 435–520). Tucson: University of Arizona Press.

Smith, B. A., Soderblom, L. A., Beebe, R. F., Boyce, J. M., Briggs, G. A., Carr, M. H., … Veverka, J. (1979b). The Galilean satellites and Jupiter: Voyager 2 imaging science results. *Science*, *206*, 927–950.

Smith, B. A., Soderblom, L. A., Johnson, T. V., Ingersoll, A. P., Collins, S. A., Shoemaker, E. M., … Suomi, V. E. (1979a). The Jupiter system through the eyes of Voyager 1. *Science*, *204*(4396), 951–972. doi:10.1126/science.204.4396.951

Sohl, F., Spohn, T., Breuer, D., & Nagel, K. (2002). Implications from Galileo observations on the interior structure and chemistry of the Galilean satellites. *Icarus*, *157*(1), 104–119. doi:10.1006/icar.2002.6828

Squyres, S. W., & Croft, S. K. (1986). The tectonics of icy satellites. *IAU Colloq. 77: Some Background about Satellites*, 293–341.

Storti, F., Holdsworth, R. E., & Salvini, F. (Eds.). (2003). *Intraplate strike-slip deformation belts*. London: Geological Society. Special Publication 210, 302pp.

Thomas, P. C. (1989). The shapes of small satellites. *Icarus*, *77*(2), 248–274.

Turcotte, D. L. (1997). *Fractals and chaos in geology and geophysics*. New York, NY: Cambridge University Press (398 pp.).

Vance, S. D., Panning, M. P., Stähler, S., Cammarano, F., Bills, B. G., Tobie, G., … Banerdt, B. (2018). Geophysical investigations of habitability in ice-covered ocean worlds. *Journal of Geophysical Research: Planets*, *122*. doi:10.1002/2017JE005341

Watters, T. R., & Schultz, R. A. (2010). *Planetary tectonics*. Cambridge: Cambridge University Press. 518 pp.

Wise, D. U., Funiciello, R., Parotto, M., & Salvini, F. (1985). Topographic lineament swarms: Clues to their origin from domain analysis of Italy. *Geological Society of America Bulletin*, *96*(7), 952–967. doi:10.1130/0016-7606(1985)96<952:TLSCTT>2.0.CO;2.

Young, R. E. (1998). The Galileo probe mission to Jupiter: Science overview. *Journal of Geophysical Research: Planets*, *103*(E10), 22775–22790.

Zahnle, K., Dones, L., & Levison, H. F. (1998). Cratering rates on the Galilean satellites. *Icarus*, *136*, 202–222.

Zahnle, K., Schenk, P., Levison, H., & Dones, L. (2003). Cratering rates in the outer Solar System. *Icarus*, *163*(2), 263–289. doi:10.1016/S0019-1035(03)00048-4